Appearance of a field-induced phase and a quantum critical line in pressurized Yb$_2$Pd$_2$Sn

N. Kabeya ®,[*] H. Komuro, N. Kimura ®, and A. Ochiai
Department of Physics, Tohoku University, Sendai 980-8578, Japan

We report three-dimensional pressure-field-temperature phase diagrams of Yb$_2$Pd$_2$Sn and Yb$_2$(Pd$_{0.9}$Ni$_{0.1}$)$_2$Sn that are constructed from electrical resistivity measurements. In Yb$_2$Pd$_2$Sn, which is known to be a pressure-induced antiferromagnet, we found an unexpected magnetic-field-induced phase at a higher field than the antiferromagnetic (AFM) phase under pressure. A non-Fermi-liquid (NFL) behavior characterized by $T^{3/2}$ dependence of the resistivity is observed along the AFM phase boundary, indicating the existence of the quantum critical line. As the AFM and field-induced phases approach each other with increasing pressure, the NFL behavior is more pronounced. Yb$_2$(Pd$_{0.9}$Ni$_{0.1}$)$_2$Sn is known to be an antiferromagnet at ambient pressure. We also found a field-induced phase under pressure. Although the temperature-pressure phase diagram of Yb$_2$(Pd$_{0.9}$Ni$_{0.1}$)$_2$Sn corresponds to that of Yb$_2$Pd$_2$Sn shifted by 1.7 GPa, the field-induced phase does not separate from the AFM phase. Furthermore, the NFL behavior is less pronounced than Yb$_2$Pd$_2$Sn. The Ni substitution for Pd not only acts as a chemical pressure but also produces other effects for the magnetism and its criticality.

I. INTRODUCTION

The peculiar phenomenon in the vicinity of the quantum critical point (QCP), at which a continuous phase transition drops to zero temperature, is firmly established as an integral part of the physics of strongly correlated electron systems. In some antiferromagnets, the nature of the QCP can be understood in terms of the Ginzburg-Landau-Wilson (GLW) framework associated with a spin-density wave (SDW) [1–5]. In this case, quantum criticality is characterized by the critical fluctuation of the antiferromagnetic (AFM) order parameter. In addition to the magnetic fluctuation, quantum critical phenomena associated with the other fluctuations, e.g., the Kondo destruction or valence fluctuation, are also intensively investigated [6–8].

These quantum critical phenomena are widely observed in a number of cerium- or ytterbium-based heavy-fermion compounds. The phenomena are often discussed based on the competition between the Kondo effect and the Ruderman-Kitte-Kasuya-Yoshida (RKKY) interaction [9]. In this model, Yb-based compounds are usually regarded as the electron-hole counterpart of Ce-based compounds. However, several asymmetric properties are found in Yb-based compounds. Some Yb-based compounds exhibit anomalous quantum critical behavior qualitatively different from that of the conventional SDW-type QCP [10–13]. In addition, magnetic properties in Yb-based compounds are robust against pressure compared with that in Ce-based compounds. This asymmetry is originated from the opposite pressure dependences of the c-f hybridization and $4f$ hole level. In principle, these pressure dependences can lead to a pressure-induced paramagnetic phase in an extreme case. Indeed, a domelike ordered phase in the pressure-temperature (P-T) phase diagram is reported in the current interest compound of Yb$_2$Pd$_2$Sn [14,15].

Yb$_2$Pd$_2$Sn crystallizes in Mo$_2$FeB$_2$-type structure with the space group $P4/mbm$ (No. 127). Yb ions form in a particular arrangement, referred to as a Shustry-Shutherland lattice, yielding geometrical frustration. The ground state is paramagnetic (PM) with a large Sonmmerford coefficient $\gamma = 560$ mJ/K^2 Yb-mol [16,17]. The electrical resistivity shows a linear temperature dependence between 0.5 and 1 K [14], which implies a quantum criticality of this compound. The valence of the Yb ion is estimated to be $\sim$+2.9 from the x-ray absorption and x-ray emission spectroscopy measurements, indicating that a strong c-f hybridization is realized [18,19]. The c-f hybridization is also evidenced by the broad maximum in the resistivity $\sim$10 K. The AFM ordered phase is induced by an application of the hydrostatic pressure up to $\sim$1 GPa but is suppressed at $\sim$4 GPa [14,15]. Note that no structural transition has been found up to 10 GPa, at least at room temperature [20]. The AFM phase forms a dome shape that appears only between 1 and 4 GPa in the P-T phase diagram. The dome-shaped AFM phase is expected to have two QCPs. However, the nature of these QCPs is not clear. Furthermore, considering that the magnetic field generally suppresses the AFM order, the two QCPs are expected to meet at a finite field. However, the behavior of this unique AFM phase in magnetic fields has not been investigated significantly.

In this paper, we report the resistivity under the fixed pressures for Yb$_2$Pd$_2$Sn and a Ni-substituted compound Yb$_2$(Pd$_{0.9}$Ni$_{0.1}$)$_2$Sn to investigate the quantum critical phenomena of these compounds. It is known that the AFM is observed at ambient pressure in Yb$_2$(Ni$_{1-x}$Pd$_x$)$_2$Sn for $x > 0.1$ [17]. The appearance of the antiferromagnetism is under-

stood as a result of lattice contraction due to the substitution as a chemical pressure. To compare the effects of the substitution and the hydrostatic pressure and to extend the experimental pressure range, we used $Yb_2(Pd_{0.9}Ni_{0.1})_2Sn$, which shows the AFM order at $T_N = 0.95$ K [17]. From the resistivity measurements, we made a pressure-field-temperature (P-H-T) phase diagram for each compound. The obtained phase diagrams of both compounds, however, are different from what was expected from the previous results. Furthermore, we found an indication of an unexpected quantum criticality under the magnetic field in Yb_2Pd_2Sn, which suggests the existing of another QCP located at a finite field.

II. EXPERIMENTAL METHOD

Single-crystalline samples of Yb_2Pd_2Sn and $Yb_2(Pd_{0.9}Ni_{0.1})_2Sn$ were grown from stoichiometric amounts of pure elements as described previously [17]. Hydrostatic pressures up to 3.07 GPa were applied using a NiCrAl-CuBe piston-cylinder cell [21]. For a pressure transmitting medium, a mixture of 1- and 2-propanol was used. The mixture keeps the liquid state up to 4 GPa at room temperature, guaranteeing a high hydrostatic pressure [22]. Both of the samples were sealed in an identical pressure cell. The pressures at low temperatures were determined from the resistivity of a manganin wire calibrated against the ac-susceptibility drop of the superconducting transition of tin [23]. The electrical resistivity was measured using a conventional four-wire method with spot-welded gold wires as terminals. Ac and dc techniques were utilized for the temperature ranges from 0.05 to 2 K and from 1.4 to 300 K, respectively. For the dc technique, a precision current source (Model 6220, Keithley, Inc.) and a nanovoltmeter (Model 2182, Keithley, Inc.) were utilized. For the ac technique, the small voltage drop in the samples was detected by a lock-in amplifier (SR830, Stanford Research Systems, Inc.) after being amplified by a precision amplifier (SA-400F3, NF Corp.). The current was carefully determined to avoid a self-heating; for instance, 0.1 mA was adopted at 0.1 K. The direction of the electrical current was along the crystallographic c axis. The magnetic field was applied along the crystallographic a axis.

III. RESULTS

We show the temperature dependences of the electrical resistivity $\rho(T)$ of Yb_2Pd_2Sn and $Yb_2(Pd_{0.9}Ni_{0.1})_2Sn$ at several fixed pressures in Fig. 1. For Yb_2Pd_2Sn, a PM ground state at 0.16 GPa is evidenced by a monotonous increase of the resistivity down to 0.05 K. As shown in the inset, the resistivity exhibits a broad peak at $T_{max} = 15$ K. This is a manifestation of the forming of the coherent Kondo state, which is consistent with the specific heat measurement [17]. Increasing pressure shifts T_{max} to lower temperatures. At 1.49 GPa, the resistivity changes in slope at $T_N = 0.66$ K, indicating the AFM transition. Here, T_N is defined as the peak temperature of the second derivative of the resistivity $d^2\rho/dT^2$. The anomaly at T_N becomes more apparent and shifts to higher temperatures with increasing pressure. Above 2.10 GPa, the shape of the anomaly changes to a hump structure. The hump implies that the Fermi surface partially disappears at T_N, which leads to a
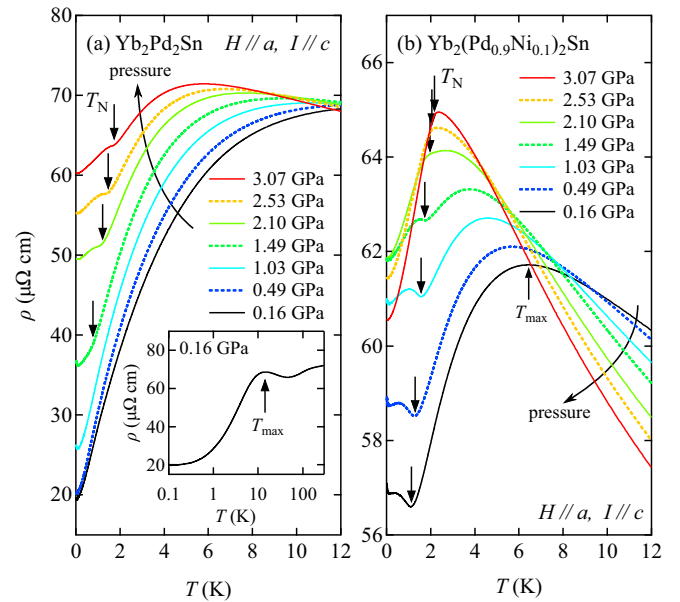

FIG. 1. Temperature dependence of the resistivity $\rho(T)$ in (a) Yb_2Pd_2Sn and (b) $Yb_2(Pd_{0.9}Ni_{0.1})_2Sn$ under several pressures. The straight arrow indicates the antiferromagnetic phase transition temperature T_N. The inset shows the resistivity of Yb_2Pd_2Sn at 0.16 GPa on the logarithmic temperature scale. The upward arrow indicates the maximum temperature T_{max} of $\rho(T)$.

decrease in the number of conduction electrons. As a result, the residual resistivity (ρ_0) increases with the appearance of antiferromagnetism.

$Yb_2(Pd_{0.9}Ni_{0.1})_2Sn$ exhibits two anomalies in the resistivity at T_N and T_{max}, even in the pressure of 0.16 GPa. As shown in Fig. 1(b), both anomalies are like those of Yb_2Pd_2Sn at high pressures. Note that we confirmed that T_N corresponds to the AFM transition temperature from the specific heat and the susceptibility measurements [17]. The peak temperature $T_{max} \sim 6$ K at 0.16 GPa is lower than that of Yb_2Pd_2Sn at the same pressure. This indicates a lower Kondo temperature than that of Yb_2Pd_2Sn. Like Yb_2Pd_2Sn, applying pressure increases T_N and decreases T_{max} in $Yb_2(Pd_{0.9}Ni_{0.1})_2Sn$. These two characteristic temperatures seem to meet at 2.53 GPa. This means the Kondo screening energy becomes comparable with the AFM ordering energy. Above 2.53 GPa, the anomaly in the resistivity at T_N changes from dip to kink. The magnetic field dependences of the resistivity, magnetoresistivity $\rho(H)$ at 0.2 K, and its field derivative $d\rho/dH$ are shown in Fig. 2. In Yb_2Pd_2Sn, the enhancement of the residual resistivity is suppressed by the magnetic field, as shown in Fig. 2(a), which is attributed to the transition from the AFM to the PM phases. Therefore, we can define a negative peak position of $d\rho/dH$ as the AFM critical field H_N, as shown in Fig. 2(c). The anomaly at H_N becomes apparent, and H_N increases with increasing pressure. At 0.16 GPa, $\rho(H)$ shows the broad maximum at $H_{max} \sim 8$ T. Here, H_{max} decreases with increasing pressure. The broad peak develops >2.53 GPa, and $\rho(H)$ forms a convex structure below the peak field. The convex structure is attributed to the emergence of another phase which is neither the PM phase nor the AFM phase. This new phase will be discussed in detail in Sec. IV. As shown in Fig. 2(c),
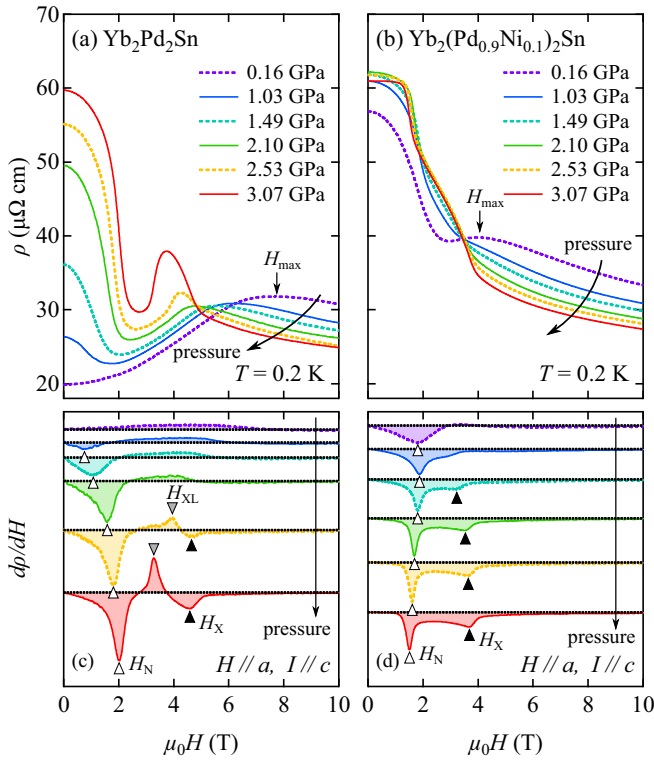
FIG. 2. Magnetoresistivity $\rho(H)$ at 0.2 K and its field derivative $d\rho/dH$ under several pressures. The white, gray, and black triangles indicate peak fields of $d\rho/dH$ named H_N, H_{XL}, and H_X, respectively. The zero value of $d\rho/dH$ for each plot is drawn as a dotted line.

a pair of the positive and negative peaks of $d\rho/dH$ appears on the lower and upper sides of the convex structure. We define the positive (negative) peak field as H_{XL} (H_X) to capture the boundaries. Although a broad positive peak can also be found <2.10 GPa, we have not assigned it as H_{XL} because the negative peak is not observed.

Field dependence of the resistivity of $Yb_2(Pd_{0.9}Ni_{0.1})_2Sn$ at low pressures is like that of Yb_2Pd_2Sn at high pressures, as shown in Fig. 2(b). For example, $\rho(H)$ of $Yb_2(Pd_{0.9}Ni_{0.1})_2Sn$ at 0.16 GPa has similar behavior to that of Yb_2Pd_2Sn at 2.10 GPa. We also observed H_N and H_{max} in $Yb_2(Pd_{0.9}Ni_{0.1})_2Sn$. While H_N increases and H_{max} decreases with increasing pressure, as seen in Yb_2Pd_2Sn, the convex structure is not obvious in $Yb_2(Pd_{0.9}Ni_{0.1})_2Sn$. We cannot recognize a positive peak in $d\rho/dH$, as shown in Fig. 2(d). Instead, we can see a shoulder anomaly in $\rho(H)$ >1.03 GPa. This result suggests the absence of H_{XL} in $Yb_2(Pd_{0.9}Ni_{0.1})_2Sn$, which means that the field-induced phase continuously appears near the AFM phase. This is a remarkable difference between Yb_2Pd_2Sn and $Yb_2(Pd_{0.9}Ni_{0.1})_2Sn$. In subsequent paragraphs, we will focus on the phase diagram and electronic state of Yb_2Pd_2Sn in relation to the presence of H_{XL}.

Figure 3 shows the temperature dependence of $d^2\rho/dT^2$ in Yb_2Pd_2Sn at some fields under selected pressures. Each plot is shifted by an amount proportional to the magnetic field to facilitate comparison with the temperature-field phase diagrams. At 2.10 GPa, where no H_{XL} or H_X is observed, the peak of $d^2\rho/dT^2$ is observed only in low fields. This
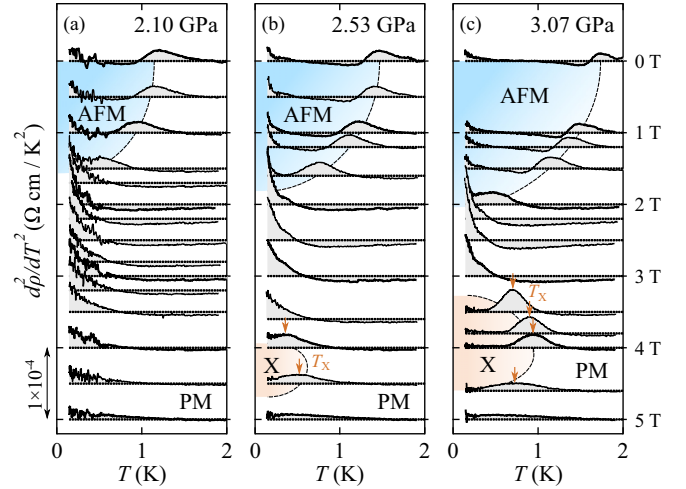

FIG. 3. Second derivative of the resistivity $d^2\rho/dT^2$ as a function of temperature in Yb_2Pd_2Sn at several pressures and fields. The arrow indicates a peak temperature T_X. Each plot is vertically shifted by an amount proportional to the measured field, where the field is indexed in the right axis. The horizontal-zero line is drawn as a dotted line.

peak is attributed to the AFM transition at $T_N(H)$. Here, T_N is suppressed to zero temperature at ~1.5 T, which is consistent with the result in Fig. 2(c). No peak appears above 1.5 T, but the value of $d^2\rho/dT^2$, namely, the coefficient A in $\rho(T) = \rho_0 + AT^2$, at low temperatures becomes large. It is gradually suppressed by further increase of the field. At 2.53 GPa, T_N shifts to a higher temperature, and H_N also shifts to a higher field. The value of $d^2\rho/dT^2$ at the lowest temperature at the fields between 2 and 3.6 T is larger than those of 2.10 GPa. At 4 and 4.5 T, it decreases rapidly, and another peak appears at T_X. Around these fields, the positive (negative) peak at H_{XL} (H_X) in $\rho(H)$ is observed (Fig. 2). Here, we define an area surrounded by T_X, H_{XL}, and H_X as phase X because we can distinguish this area clearly in both $\rho(T)$ and $\rho(H)$. At 3.07 GPa, the peak at T_X becomes more apparent, and the phase X expands as well as the AFM phase does. Hence, the AFM and X phases approach each other.

The detailed results of Yb_2Pd_2Sn at 3.07 GPa are shown in Fig. 4. The convex structure in $\rho(H)$ is smeared out with increasing temperature. Instead, a shoulder structure appears, as shown in Fig. 4(a). The curve shape of $\rho(H)$ >1 K is quite like that of $Yb_2(Pd_{0.9}Ni_{0.1})_2Sn$ at 0.2 K >2 GPa. As shown in the inset of Fig. 4(a), the temperature variation of $\rho(H)$ curves in $Yb_2(Pd_{0.9}Ni_{0.1})_2Sn$ is smaller than that in Yb_2Pd_2Sn. These results imply that the atomic replacement yields a similar effect of thermal fluctuations.

As expected from the temperature evolution of the magnetoresistivity, $\rho(T)$ at low temperatures strongly depends on the field, as shown in Fig. 4(b). For instance, $\rho(T)$ between 2 and 3 T, where $H_N < H < H_{XL}$, exhibits a steeper slope at low temperatures, while $\rho(T)$ at 4 T, where $H_{XL} < H < H_X$, shows very weak-temperature dependence below $T_X \sim 1$ K. To evaluate temperature dependence of $\rho(T)$, we plotted the field dependence of the coefficient A at low temperatures, as shown in Fig. 4(c). We found that A strongly depends on
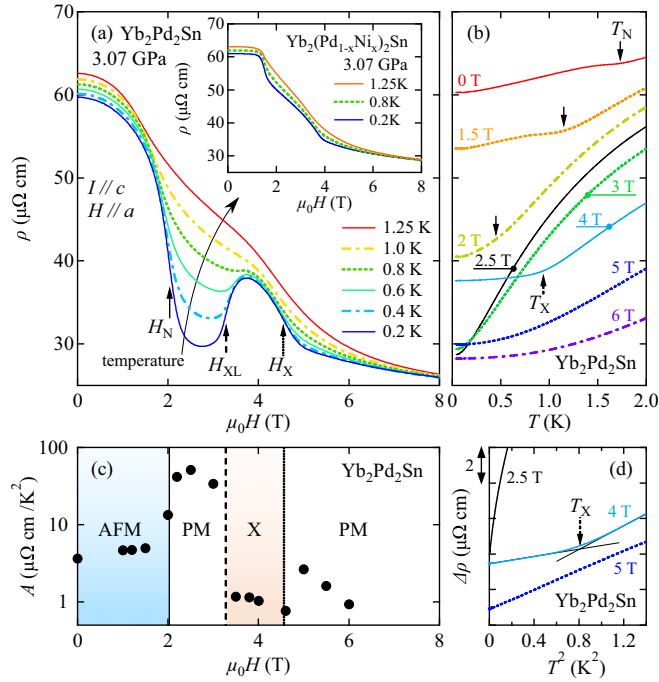
FIG. 4. Resistivity and its squared-temperature coefficient A of Yb_2Pd_2Sn at 3.07 GPa. (a) and (b) The field and temperature dependence of the resistivity, respectively. The inset of the panel (a) shows the magnetoresistivity of $Yb_2(Pd_{0.9}Ni_{0.1})_2Sn$ at 3.07 GPa. (c) Field dependence of A. Vertical lines correspond to H_N, H_{XL}, and H_X on $d\rho/dH$ at 0.2 K. (d) Squared-temperature dependence of the resistivity of Yb_2Pd_2Sn at 3.07 GPa.

the magnetic field. It changes steeply at H_N, H_{XL}, and H_X. These discontinuous changes of A suggest phase transitions at those fields. Another remarkable point is that the value of A at $H_N < H < H_{XL}$ is >10 times larger than those at other fields. The significant enhancement of A indicates strong fluctuations, probably due to the quantum criticality in the vicinity of 2.5 T at 3.07 GPa in Yb_2Pd_2Sn. In contrast, at a field for $H_{XL} < H < H_X$, the value of A is small compared with that in the surrounding PM phases. As shown in Fig. 4(d), an abrupt change of the slope on $\rho(T)$ implies a drastic change of the electronic structure at T_X.

IV. DISCUSSION

In the $Yb_2(Pd_xNi_{1-x})_2Sn$ system, the AFM order is induced by pressure as well as Ni substitution for Pd [15,17]. The Ni substitution is expected to affect as a chemical pressure, that is, it reduces the lattice constant because Ni has a smaller ionic radius than Pd. Unfortunately, we cannot determine the lattice constants of Yb_2Pd_2Sn and $Yb_2(Pd_{0.9}Ni_{0.1})_2Sn$ under pressure. Then we attempt to estimate the magnitude of the chemical pressure due to 10% of Ni substitution by superimposing the pressure dependence of T_N in Yb_2Pd_2Sn and $Yb_2(Pd_{0.9}Ni_{0.1})_2Sn$. Figure 5 shows the pressure dependence of T_N, T_{max}, and ρ_0. When we shift the origin of the pressure axis for $Yb_2(Pd_{0.9}Ni_{0.1})_2Sn$ (top axis) by +1.7 GPa from that for Yb_2Pd_2Sn (bottom axis), the viewgraphs of T_N of both compounds almost overlap.

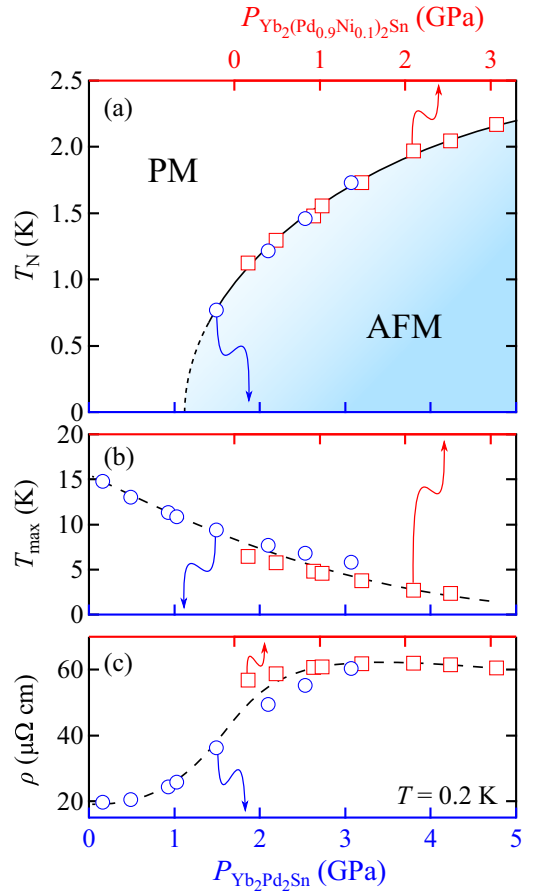FIG. 5. Pressure dependence of (a) T_N, (b) T_{max}, and (c) ρ_0. The pressure scales for Yb_2Pd_2Sn and $Yb_2(Pd_{0.9}Ni_{0.1})_2Sn$ are drawn on the bottom and top axes, respectively. The origin of the scale for $Yb_2(Pd_{0.9}Ni_{0.1})_2Sn$ is shifted by +1.7 GPa from the scale for Yb_2Pd_2Sn.

Therefore, we estimate that the chemical pressure is equivalent to 1.7 GPa. Similar correspondences are also obtained in T_{max} and ρ_0, as shown in Figs. 5(b) and 5(c). These results suggest that the Ni substitution works as a chemical pressure. However, as shown in Fig. 2 (see also Fig. 6), the qualitative difference of the magnetic field responses between Yb_2Pd_2Sn and $Yb_2(Pd_{0.9}Ni_{0.1})_2Sn$ indicates that the Ni substitution does not have just a chemical pressure effect.

The pressure dependence of T_N in Fig. 5(a) is qualitatively different from the previous study in which T_N of polycrystalline Yb_2Pd_2Sn peaks at ~2 GPa and the P-T phase diagram constructs the dome-shaped AFM phase [14,15]. In this paper, T_N of both single-crystalline Yb_2Pd_2Sn and $Yb_2(Pd_{0.9}Ni_{0.1})_2Sn$ increases monotonically with increasing pressure up to 3 GPa. Note that, in general, anomaly and ordering temperature of a long-range order tend to be smeared out and suppressed, respectively, in polycrystalline samples. This is one possible reason for the qualitative difference. Our results indicate that an application of pressure stabilizes the AFM ground state. A similar monotonic dependence is also found in T_{max}, shown in Fig 5(b), which suggests that the Kondo temperature T_K that scales itinerancy of 4f electrons is suppressed at higher pressures. This is consistent with the
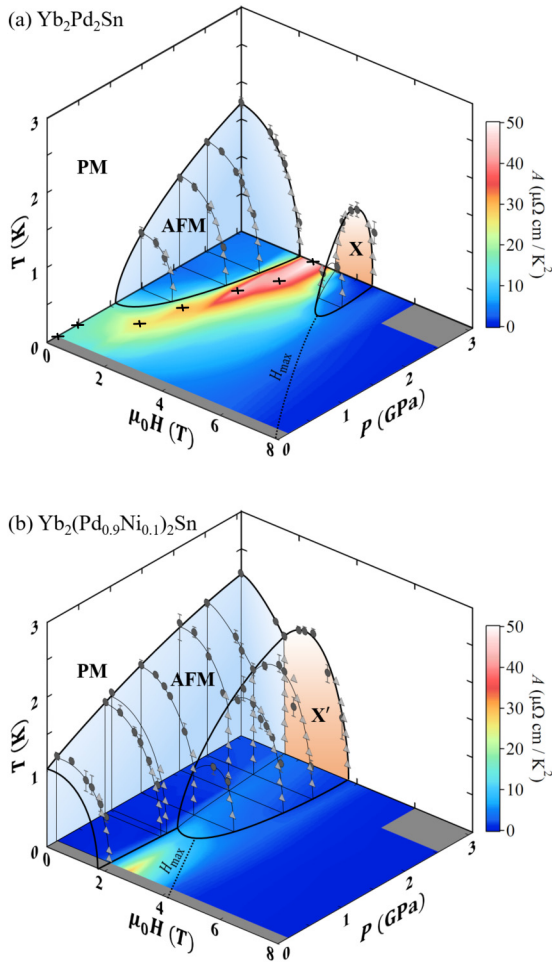
(a) Yb$_2$Pd$_2$Sn

(b) Yb$_2$(Pd$_{0.9}$Ni$_{0.1}$)$_2$Sn

FIG. 6. Three-dimensional pressure-field-temperature phase diagrams of (a) Yb$_2$Pd$_2$Sn and (b) Yb$_2$(Pd$_{0.9}$Ni$_{0.1}$)$_2$Sn. The right-hand back plane corresponds to the field-temperature phase diagram at 3.07 GPa. The contour map on the bottom plane represents the T^2 coefficient A of the resistivity obtained from a fit for $\rho(T) = \rho_0 + AT^2$. The cross mark indicates the position of the magnetic field and pressure at which the data in Fig. 7 were taken.

FIG. 7. Temperature dependence of the resistivity of Yb$_2$Pd$_2$Sn for the selected fields at which the A coefficient becomes the maximum in each pressure. The temperature scaling in each panel is (a) linear, (b) $T^{3/2}$, and (c) squared. Solid lines are guide for eyes.

pressure dependence of T_N because suppression of the itinerancy of $4f$ electrons induces magnetic order.

To summarize the temperature, field, and pressure dependences of the resistivity, we construct three-dimensional P-H-T phase diagrams of Yb$_2$Pd$_2$Sn and Yb$_2$(Pd$_{0.9}$Ni$_{0.1}$)$_2$Sn, as shown in Fig. 6. Yb$_2$Pd$_2$Sn has the AFM and X phases in addition to the PM phase. The X phase appears as an extension of the H_{max} and is not in contact with the AFM phase in the present parameter range. In addition, it is surrounded by a closed boundary. Therefore, the transition between the PM and X phases may involve symmetry breaking because the symmetry breaking cannot become a crossover. The contour map on the bottom plane displays the value of A obtained by forcibly fitting the data to the equation $\rho(T) = \rho_0 + AT^2$. We selected a temperature range, typically $T < 0.3$ K, that allows us to adapt the data to this equation within an experimental error. Note that the filling of the contour map in Fig. 6 does not mean that the T^2 behavior persists in the entire area of the map. The temperature exponent in the resistivity will be
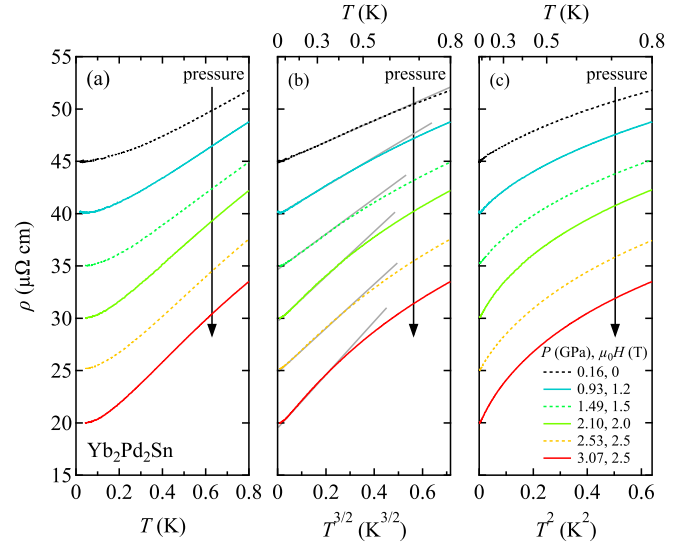
discussed later. Here, A shows large values around the AFM phase, which becomes more pronounced with increasing pressure.

Like Yb$_2$Pd$_2$Sn, Yb$_2$(Pd$_{0.9}$Ni$_{0.1}$)$_2$Sn has the AFM, X$'$, and PM phases. Here, we will distinguish the X$'$ phase from the X phase thus far because they have not been identified yet. In contrast to the X phase, the X$'$ phase appears attached to the AFM phase. As the pressure increases, the regions of both AFM and X$'$ phases expand, and the overlap becomes stronger. The enhancement of the A value is observed in a rather lower pressure side for Yb$_2$(Pd$_{0.9}$Ni$_{0.1}$)$_2$Sn.

The phase diagrams of Yb$_2$Pd$_2$Sn and Yb$_2$(Pd$_{0.9}$Ni$_{0.1}$)$_2$Sn clearly differ in two aspects. One is that the X$'$ phase is in contact with the AFM phase, but the X phase is not. The other is that a strong divergence of the A value is observed around the AFM phase in Yb$_2$Pd$_2$Sn but not in Yb$_2$(Pd$_{0.9}$Ni$_{0.1}$)$_2$Sn. These two differences are probably related because A is strongly suppressed in the X and X$'$ phases, as shown in the bottom plane of Fig. 6 and in Fig. 4(c). The differences in the phase diagrams suggest that atomic substitution produces more than just chemical pressure. Atomic substitution not only changes the distance to the surrounding elements but also induces a local distortion. Such a distortion may not significantly change the Fermi surface but has potential to suppress the fluctuations induced by the geometrical frustration and/or valence change. Thus, the stronger fluctuations in Yb$_2$Pd$_2$Sn may retain the X phase apart from the AFM phase, while the weaker fluctuations, realized in Yb$_2$(Pd$_{0.9}$Ni$_{0.1}$)$_2$Sn, allow the X$'$ phase to approach the AFM phase.

The enhancement of A suggests a large amount of the excitation of quasiparticles at low temperatures. The temperature exponent of the resistivity reflects the properties of the excitation. To evaluate the exponent of the resistivity, we picked up the resistivity of Yb$_2$Pd$_2$Sn at the field where the coefficient A is the largest at each pressure in Fig. 7. Note that the corresponding combination of pressure and field is indicated

by the cross mark in Fig. 6(a). We can see that the resistivity at each pressure and field shows good linearity in the $T^{3/2}$ plot. According to the self-consistent renormalization theory in the GLW framework, this temperature exponent is expected from three-dimensional AFM fluctuation [4]. Therefore, this fluctuation is attributed to AFM quantum criticality. The observations of large A and $T^{3/2}$ dependence in the resistivity along the AFM-PM phase boundary strongly suggest that the phase boundary at 0 K is a quantum critical line (QCL).

Next, we turn to discuss the phase X of Yb_2Pd_2Sn. The X phase is characterized by the weak temperature dependence of $\rho(T)$, relatively large ρ_0, and closed boundary between the PM phase. The small A and large ρ_0 can be interpreted as the results of the partial loss of the Fermi surface that has a rather heavy effective mass. This situation is possibly induced by the nesting of the Fermi surface, which is attributed to density waves such as the SDW or charge density wave. Such a field-induced SDW has been reported for an unusual field-induced phase (A phase) of $Sr_3Ru_4O_7$ [24]. In the A phase, ρ shows a larger residual value and a weaker temperature dependence than around phases [25]. Furthermore, the A phase locates in the vicinity of the metamagnetic QCP. These similarities may imply a possibility of a field-induced SDW in the X phase of Yb_2Pd_2Sn.

The phase boundaries of the AFM and X phases at zero temperature will contact at ∼4 GPa if we linearly extrapolate them to higher pressures. The value of A is enhanced toward higher pressures and possibly diverges at the contact point. Therefore, the contact point may have a stronger and possibly different criticality than that of the QCL. One candidate for the contact point is a quantum bicritical point (QBCP), as discussed in Ref. [26]. The QBCP is the point at which two different QCLs meet. In this paper, one QCL is of the AFM phase, and the other should be of the X phase. However, the critical behavior is not observed around the phase boundary of the X phase in Yb_2Pd_2Sn. Of course, since we have not identified the order parameter of the X phase, its critical behavior may be different from our expectation. Therefore, we do not exclude the possibility of the contact point being

the QBCP. To elucidate why the value of A rapidly enhances toward the contact point, we are conducting thermodynamical experiments in higher pressures.

V. CONCLUSIONS

We have investigated the *P-H-T* phase diagrams and the quantum critical phenomena of Yb_2Pd_2Sn and $Yb_2(Pd_{0.9}Ni_{0.1})_2Sn$ by measuring the electrical resistivity under pressures and magnetic fields. As for $H = 0$, the substitution of Ni for Pd acts as chemical pressure. For $H \neq 0$, we found the field-induced X and X' phases in Yb_2Pd_2Sn and $Yb_2(Pd_{0.9}Ni_{0.1})_2Sn$ in the higher field region of the AFM phase. The X and X' phases are closed and characterized by a small A value. In Yb_2Pd_2Sn, the X phase is separated from the AFM phase. Around the AFM phase, $\rho(T)$ exhibits $T^{3/2}$ dependence, indicating that the boundary between the AFM and PM phases in the $T = 0$ plane is the QCL. The divergent tendency of the A value toward the contact point of the AFM and X phases is observed. On the other hand, $Yb_2(Pd_{0.9}Ni_{0.1})_2Sn$ shows that the X' phase connects to the AFM phase. The enhancement of the A value is rather weak around the contact point of these phases. The difference between these compounds may result from the local distortion induced by the atomic substitution. Investigating the divergent tendency of the A value and development of the X phase toward higher pressures would improve our understanding of the anomalous quantum critical behaviors in not only Yb-based compounds but also $4f$ electron systems involving the duality of the itinerant and localized feature. One avenue of future work would be to compare the quantum criticality in finite fields with other pressure-induced antiferromagnets.

[1] J. A. Hertz, Phys. Rev. B **14**, 1165 (1976).

[2] A. J. Millis, Phys. Rev. B **48**, 7183 (1993).

[3] T. Moriya and T. Takimoto, J. Phys. Soc. Jpn. **64**, 960 (1995).

[4] T. Moriya and K. Ueda, Rep. Prog. Phys. **66**, 1299 (2003).

[5] G. R. Stewart, Rev. Mod. Phys. **73**, 797 (2001).

[6] J. H. Pixley, S. Kirchner, K. Ingersent, and Q. Si, Phys. Rev. Lett. **109**, 086403 (2012).

[7] S. Watanabe and K. Miyake, Phys. Rev. Lett. **105**, 186403 (2010).

[8] S. Watanabe and K. Miyake, J. Phys.: Condens. Matter **23**, 094217 (2011).

[9] S. Doniach, Physica **91B**, 231 (1977).

[10] P. Gegenwart, J. Custers, C. Geibel, K. Neumaier, T. Tayama, K. Tenya, O. Trovarelli, and F. Steglich, Phys. Rev. Lett. **89**, 056402 (2002).

[11] Y. Matsumoto, S. Nakatsuji, K. Kuga, Y. Karaki, N. Horie, Y. Shimura, T. Sakakibara, A. H.

Nevidomskyy, and P. Coleman, Science **331**, 316 (2011).

[12] K. Deguchi, S. Matsukawa, N. K. Sato, T. Hattori, K. Ishida, H. Takakura, and T. Ishimasa, Nat. Mater. **11**, 1013 (2012).

[13] K. Matsubayashi, T. Hirayama, T. Yamashita, S. Ohara, N. Kawamura, M. Mizumaki, N. Ishimatsu, S. Watanabe, K. Kitagawa, and Y. Uwatoko, Phys. Rev. Lett. **114**, 086401 (2015).

[14] E. Bauer, H. Michor, T. Muramatsu, T. Kanemasa, T. Kagayama, K. Shimizu, Y. Aoki, H. Sato, and M. Giovannini, J. Optoelectron. Adv. Mater. **10**, 1633 (2008).

[15] T. Muramatsu, T. Kanemasa, T. Kagayama, K. Shimizu, Y. Aoki, H. Sato, M. Giovannini, P. Bonville, V. Zlatic, I. Aviani, R. Khasanov, C. Rusu, A. Amato, K. Mydeen, M. Nicklas, H. Michor, and E. Bauer, Phys. Rev. B **83**, 180404(R) (2011).

[16] E. Bauera, G. Hilschera, H. Michora, C. Paula, Y. Aokib, and H. S. and, J. Magn. Magn. Mater. **272–276**, 237 (2004).

[17] F. Kikuchi, K. Hara, E. Matsuoka, H. Onodera, S. Nakamura, T. Nojima, K. Katoh, and A. Ochiai, J. Phys. Soc. Jpn. **78**, 083708 (2009).

[18] E. Bauer, G. Hilscher, H. Michor, C. Paul, Y. Aoki, H. Sato, D. T. Adroja, J.-G. Park, P. Bonville, C. Godart, J. Sereni, M. Giovannini, and A. Saccone, J. Phys.: Condens. Matter **17**, S999 (2005).

[19] H. Yamaoka, P. Thunström, N. Tsujii, I. Jarrige, K. Shimada, M. Arita, H. Iwasawa, H. Hayashi, J. Jiang, H. Namatame, M. Taniguchi, N. Hiraoka, H. Ishii, K.-D. Tsuei, M. Giovannini, and E. Bauer, Phys. Rev. B **86**, 085137 (2012).

[20] G. Lamura, I. J. Onuorah, P. Bonfà, S. Sanna, Z. Shermadini, R. Khasanov, J.-C. Orain, C. Baines, F. Gastaldo, M. Giovannini, I. Čurlík, A. Dzubinska, G. Pristas, M. Reiffers, A. Martinelli,

C. Ritter, B. Joseph, E. Bauer, R. De Renzi, and T. Shiroka, Phys. Rev. B **101**, 054410 (2020).

[21] Y. Uwatoko, S. Todo, K. Ueda, A. Uchida, M. Kosaka, N. Mori, and T. Matsumoto, J. Phys.: Condens. Matter **14**, 11291 (2002).

[22] G. J. Piermarini, S. Block, and J. D. Barnett, J. Appl. Phys. **44**, 5377 (1973).

[23] L. D. Jennings and C. A. Swenson, Phys. Rev. **112**, 31 (1958).

[24] C. Lester, S. Ramos, R. S. Perry, T. P. Croft, R. I. Bewley, T. Guidi, P. Manuel, D. D. Khalyavin, E. M. Forgan, and S. M. Hayden, Nat. Mater. **14**, 373 (2015).

[25] P. Gegenwart, F. Weickert, M. Garst, R. S. Perry, and Y. Maeno, Phys. Rev. Lett. **96**, 136402 (2006).

[26] Y. Tokiwa, M. Garst, P. Gegenwart, S. L. Bud'ko, and P. C. Canfield, Phys. Rev. Lett. **111**, 116401 (2013).